

Solving partial differential equations in quantum computers

Paula García-Molina, Javier Rodríguez-Mediavilla, and Juan José García-Ripoll

Instituto de Física Fundamental, IFF-CSIC, Calle Serrano 113b, 28006 Madrid, Spain

In this work, we develop a variational quantum algorithm to solve partial differential equations (PDE's) using a space-efficient variational ansatz that merges structured quantum circuits for coarse-graining with Fourier-based interpolation. We implement variational circuits to represent symmetrical smooth functions as the ansatz and combine them with classical optimizers that differ on the gradient calculation: no gradient, numerical gradient and analytic gradient. We apply this method to the computation of the ground state of the one-dimensional quantum harmonic oscillator and the transmon qubit. In idealized quantum computers, we show that the harmonic oscillator can be solved with an infidelity of order 10^{-5} with 3 qubits and the transmon qubit with an error of order 10^{-4} with 4 qubits. We find that these fidelities can be approached in real noisy quantum computers, either directly or through error mitigation techniques. However, we also find that the precision in the estimate of the eigenvalues is still sub-par with other classical methods, suggesting the need for better strategies in the optimization and the evaluation of the cost function itself.

1 Introduction

Early at the beginning of quantum computing, one of the suggested applications was the encoding and manipulation of discretized functions [1, 2], as states of the quantum register. This idea opens the field of *quantum numerical analysis*, where quantum computers assist in tasks such as the solution of linear, nonlinear and differential equations. In 2006, Kacewicz demonstrated a quantum speed up in the solution of initial-

value problems for ordinary differential equations (ODE's) [3], using quantum amplitude estimation as a subroutine of a classical method. In 2008, Leyton and Osborne [4] suggested using quantum computers to solve nonlinear ordinary differential equations. Unlike an earlier work by Kacewicz [3]—later adapted to the Navier-Stokes partial differential equations (PDE's) [5]—, the quantum computer is not a subroutine in a classical method, but the whole problem is encoded in the quantum computer. In 2014, Berry [6] pushed this idea forward, transporting the quantum speedups of the HHL [7] for linear systems of equations, to the solution of ODE's, by means of the Euler method and quantum simulation. Since then, a great deal of effort has been put into this technique, improving its precision [8] and extending the method to PDE's [9]. This technique also suits the finite element method [10] and spectral methods [11], as well as a variety of linear problems—the Poisson equation [12], the heat equation [13] or the wave equation [14], which is successfully simulated in Ref. [15]. Such ideas, in combination with the Carleman [16] or the quantum nonlinear Schrödinger linearization [17], can also be applied to weakly nonlinear differential equations. Note also alternative methods based on hardware-efficient Taylor expansions [18], or on the intrinsic dynamics provided by continuous variable quantum computers [19].

Even though HHL-based or quantum-simulation-based differential equation solvers exhibit potential quantum speedups, they require large numbers of qubits and operations, far from current NISQ [20] devices, and closer to the specifications of fault-tolerant scalable quantum computers. In this context, variational hybrid quantum-classical algorithms [21] appeared as a family of methods with lower hardware requirements and strong resilience to noise [22], more adequate to the state of the art. In this paradigm, a variational quantum circuit encodes the solution to a complex problem—an ODE or

Paula García-Molina: paula.garcia@iff.csic.es

PDE in our case—, and the parameters of the circuit are tuned through a *learning process* that optimizes a *loss function*. In some cases, the variational form encodes the complete function [23, 24], while in others the variational circuit acts as a quantum neural network that, given the right coordinates, outputs a prediction for the function under study [25, 26]. The resulting algorithms have a wide range of applications, including physics [27], chemistry [28], and finance [29], and may work both with non-unitary [24, 29] and nonlinear differential equations [23].

In this work we introduce a variational quantum algorithm for solving static PDE’s, that relies on the quantum Fourier transform and the quantum Fourier interpolation algorithm [30], and works also with a new type of variational ansätze, that takes into account symmetries and a smoother encoding of differentiable functions. Our study focuses on the impact of finite-precision and gate errors in the estimation of the cost function, and how this affects the estimation of the solution and the eigenvalues themselves. Surprisingly, we find that the variational algorithm exhibits a great performance, achieving an error $1 - F^\infty = 10^{-5} - 10^{-4}$ in the solution of the harmonic oscillator and the transmon qubit equations. This precision is well above what one would expect when the cost function is estimated with a finite number of measurements, and illustrates the resilience of variational methods when combined with stochastic optimization. However, our study also shows that even though the functions may be very well approximated, the actual computation of observable properties, such as the equation’s eigenvalues, may be severely limited by the finite precision of the quantum computer, demanding numbers of measurements $\sim 10^4 - 10^5$ or gate precisions that can exceed those of current NISQ computers.

The structure of this paper is as follows. In section 2 we introduce a general family of Hamiltonian PDE’s and a variational algorithm to solve them. This algorithm is specialized in section 2.1 for a particular encoding of functions in the quantum computer [1, 2]. In section 2.2 we provide three variational ansätze: a generic one based on σ^y rotations, one adapted for this function encoding, and a meta-variational circuit that symmetrizes either of those. In section 3 we introduce two equations—the quantum harmonic oscillator

and the transmon qubit—as two models that we will use to benchmark this algorithm. Section 4 discusses the application of these algorithms for the harmonic oscillator (cf. section 4.2) and for the transmon qubit (cf. section 4.3). Our study begins first with idealized quantum computers, analyzing the limitations of the algorithm, the ansatz and the optimization methods. We then simulate realistic NISQ devices in section 4.4, analyzing the attainable fidelities and introducing error mitigation techniques to improve our estimate of the PDE’s eigenvalues. Finally, in section 5 we discuss the conclusions drawn from this work and outline further research.

2 Variational quantum PDE solver

In this work we consider PDE’s of the form

$$[D(-i\nabla) + V(\mathbf{x})] f(\mathbf{x}) = Ef(\mathbf{x}), \quad (1)$$

defined over a regular domain $x_i \in [a_i, b_i]$, with periodic boundary conditions, $f(\mathbf{x} + (b_i - a_i)\mathbf{e}_i) = f(\mathbf{x})$ and real functions $D(\mathbf{p}), V(\mathbf{x}) \in \mathbb{R}$. We assume that the PDE is a lower-bounded Hamiltonian operator,

$$H = D(-i\nabla) + V(\mathbf{x}) \geq E_{\min}, \quad (2)$$

and we seek the ground state E_{\min} or lowest energy excitations. As practical examples of this type of equations, we will study the one-dimensional quantum harmonic oscillator (see section 3.1) and the transmon qubit (section 3.2).

We propose to solve this type of equations using a hybrid quantum-classical algorithm with the following ingredients (Fig. 1):

- (i) A map between states $|f^{(n)}\rangle$ of a quantum register with n qubits and bandwidth-limited continuous functions $f(\mathbf{x})$.
- (ii) The realization that given $|f^{(n)}\rangle$, the quantum Fourier transform (QFT) creates a state $|\tilde{f}^{(n)}\rangle$ that encodes the classical Fourier transform $\tilde{f} = \mathcal{F}f$ of the encoded function $f(\mathbf{x})$.
- (iii) A quantum algorithm that uses $|f^{(n)}\rangle$ and $|\tilde{f}^{(n)}\rangle$, and suitable representations of position and momentum operators $\hat{\mathbf{x}}$ and $\hat{\mathbf{p}}$, to estimate the energy functional $E[f] =$

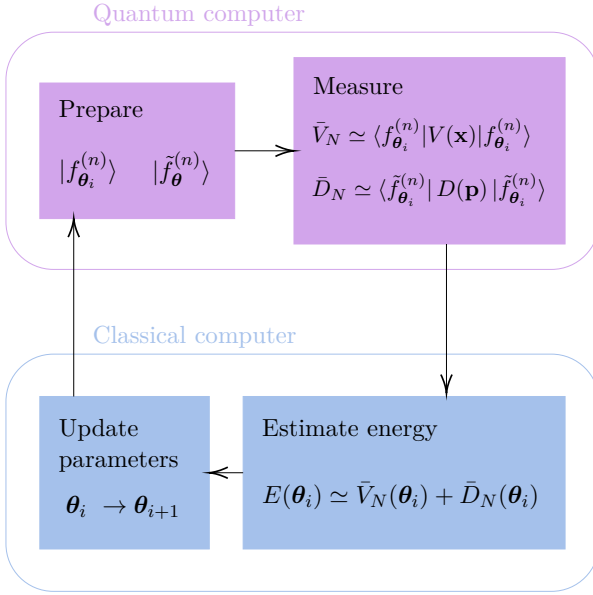


Figure 1: Variational quantum PDE solver. We use a quantum computer to initialize two quantum circuits in the states $|f_{\theta_i}^{(n)}\rangle$ and $|\tilde{f}_{\theta_i}^{(n)}\rangle$. We estimate the expectation values of the $V(\mathbf{x})$ and $D(\mathbf{p})$ operators from measurements in the quantum computer, thereby approximating the energy functional $E[\theta]$. A classical computer uses these estimates to iteratively update the parameters of the quantum variational circuit, until convergence.

(f, Hf) with polynomial resources as

$$E[f] \simeq \langle \tilde{f}^{(n)} | D(\hat{\mathbf{p}}) | \tilde{f}^{(n)} \rangle + \langle f^{(n)} | V(\hat{\mathbf{x}}) | f^{(n)} \rangle. \quad (3)$$

- (iv) A quantum variational circuit $W(\theta)$, creating parameterized states of a quantum register with n qubits $|f_{\theta}^{(n)}\rangle = W(\theta)|00\dots0\rangle$ (section 2.2).
- (v) A classical optimization algorithm, such as COBYLA, SPSA or ADAM, that given $E(\theta)$ finds the parameters θ that minimize this function.

Ideas (i) and (iv) establish a map from a set of real optimizable parameters $\theta \in \mathbb{R}^k$, to the set of bandwidth limited functions $f_{\theta}(\mathbf{x})$ and their energies $E[f_{\theta}] =: E(\theta)$. Algorithms (ii) and (iii) provide us with a quantum recipe to estimate $E(\theta)$. The classical algorithm (v) hybridizes with the quantum algorithms (i)-(iv), allowing us to search the variational function f_{θ} that best approximates a solution to Eq. (1),

$$\operatorname{argmin}_f \langle f | H | f \rangle \leq f_{\operatorname{argmin}_{\theta} E(\theta)}. \quad (4)$$

Section 2.1 provides a deeper explanation of points (ii)-(iv), while the variational forms are explained in the following section.

2.1 Working with functions in a quantum computer

2.1.1 Position space discretization

Before we address the solution of differential equations, we need to find an encoding of such functions in a quantum register. Without loss of generality, we center our discussion on one-dimensional problems. Our work assumes periodic functions or functions $f(x)$ that vanish towards the boundaries of a finite interval $[a, b]$, of size $L_x = |b - a|$. We also focus on functions that are bandwidth limited: i.e., their Fourier transform $\tilde{f}(p) = [\mathcal{F}f](p)$ is negligible outside a corresponding interval in momentum or frequency space $[-L_p/2, L_p/2]$.

To each such function $f(x)$ we associate a quantum state $|f^{(n)}\rangle$ with n qubits, discretizing the function on a regular grid with 2^n points, labeled

$$x_s^{(n)} = a + s\Delta x, \text{ with } s \in \{0, 1, \dots, 2^n - 1\} \quad (5)$$

and $\Delta x^{(n)} = \frac{L_x}{2^n}$. The discretized and normalized state is a linear superposition

$$|f^{(n)}\rangle = \frac{1}{\mathcal{N}_f^{1/2}} \sum_{s=0}^{2^n-1} f(x_s^{(n)}) |s\rangle, \quad (6)$$

of quantum register states $|s\rangle$ that encode the integer s into the states of n qubits, with a normalization constant \mathcal{N}_f that depends on the number of qubits.

The Nyquist-Shannon theorem [31, 32] ensures that any bandwidth-limited function $f(x)$ can be interpolated from a discretization $|f^{(n)}\rangle$ with spacing $\Delta x^{(n)} \leq 2\pi/L_p$, up to exponentially small errors. This allows us to (i) estimate the smallest number of qubits required to make the sampling accurate, (ii) establish the inverse mapping, from states $|f^{(n)}\rangle$ to functions, and (iii) develop an algorithm to create interpolated states $|f^{(n+m)}\rangle$ and $|\tilde{f}^{(n+m)}\rangle$ for the estimation of the wavefunction and its energy if necessary. All this follows from the next section.

2.1.2 Momentum space and Fourier interpolation

Given an n -qubit discretized function $|f^{(n)}\rangle$, we can straightforwardly implement the quantum

Fourier transform (QFT). This unitary operator $\hat{\mathcal{F}}$ is the quantum analogue of the discrete Fourier transform,

$$|r\rangle \rightarrow \frac{1}{\sqrt{2^n}} \sum_{s=0}^{2^n-1} e^{i2\pi rs/2^n} |s\rangle. \quad (7)$$

When applied on $|f^{(n)}\rangle$, $\hat{\mathcal{F}}$ produces the quantum state that encodes the discrete Fourier transform of the series of values $\{f(x_s)\}$

$$\begin{aligned} |\tilde{f}^{(n)}\rangle &= \sum_s \tilde{f}^{(n)}(p_s) |s\rangle := \hat{\mathcal{F}} |f^{(n)}\rangle \quad (8) \\ &= \frac{1}{\sqrt{2^n}} \sum_{r,s=0}^{2^n-1} e^{i2\pi sr/2^n} f(x_r) |s\rangle. \end{aligned}$$

As in the discrete Fourier transform, we have to deal with the annoying ordering of quasimomenta $p_s \in [-L_p/2, L_p/2]$ that stores negative frequencies in the higher states of the quantum register

$$p_s = \frac{2\pi}{\Delta x^{(n)} 2^n} \times \begin{cases} s, & 0 \leq s < 2^{n-1}, \\ s - 2^n, & \text{otherwise.} \end{cases} \quad (9)$$

If we work with bandwidth-limited functions and the discretization step is small enough $\Delta x^{(n)} \leq 2\pi/L_p$, we can reconstruct the original function from the discretized state in momentum space. Up to normalization, we write

$$f(x) \propto \sum_{s=0}^{2^n-1} e^{-ip_s x} \langle s | \hat{\mathcal{F}} | f^{(n)} \rangle. \quad (10)$$

This equation represents a mapping from states in the quantum register to continuous, infinitely differentiable bandwidth-limited functions. It also provides us with a recipe to interpolate the discretized function $|f^{(n)}\rangle$ up to arbitrary precision, using more qubits to represent more points in the position space.

As sketched in Fig. 2a, to perform this *position space interpolation scheme* we need three steps. First, compute the QFT of the originally encoded function $|\tilde{f}^{(n)}\rangle$. Second, add m auxiliary qubits to enlarge the momentum space. Due to the anomalous encoding of momenta (Eq. (9)), the original discretization with 2^n points must be mapped to the intervals $s \in [0, 2^{n-1}] \cup [2^{n+m} - 2^{n-1}, 2^{n+m}]$. This is done using a two's complement operation $U_{2^s c}$ where the sign of the values of the auxiliary register is determined by the most significative

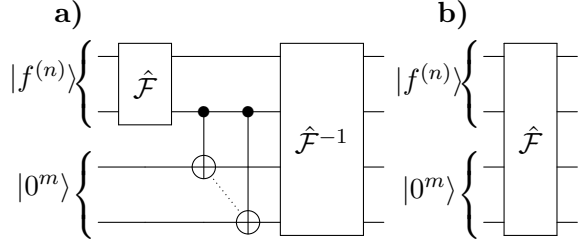


Figure 2: Quantum interpolation algorithms. (a) Algorithm to recreate a finer interpolation in position space $|f^{(n+m)}\rangle$ adding m qubits to a previous discretization $|f^{(n)}\rangle$. (b) Algorithm to recreate a momentum space discretization with $n + m$ qubits from $|f^{(n)}\rangle$.

qubit of the original register. Finally, we Fourier-transform back to recover the state with $n + m$ qubits. The complete algorithm reads

$$\begin{aligned} |f^{(n+m)}\rangle &= \hat{\mathcal{F}}^{-1} U_{2^s c} (|0\rangle^{\otimes m} \otimes \hat{\mathcal{F}} |f^{(n)}\rangle) \quad (11) \\ &=: U_{\text{int}}^{n,m} |f^{(n)}\rangle. \end{aligned}$$

We can define another, simpler *momentum space interpolation* scheme that associates $|f^{(n)}\rangle$ to a continuous, differentiable function in momentum space $\tilde{f}(p)$

$$\tilde{f}(p) \propto \sum_{s=0}^{2^n-1} e^{ipx_s} \langle s | f^{(n)} \rangle, \quad p \in [-L_p/2, L_p]. \quad (12)$$

The quantum interpolation method enlarges the number of points in momentum space by a factor 2^m using m auxiliary qubits and a quantum Fourier transform (Fig. 2b)

$$|\tilde{f}^{(n+m)}\rangle = \hat{\mathcal{F}}_{n+m} [|0\rangle^{\otimes m} \otimes |f^{(n)}\rangle]. \quad (13)$$

This is equivalent to extending the grid on which we discretize $f(x)$ from $[a, b]$ to $[a, b + 2^m L_x]$, setting all those extra points to the same value that the function takes at the boundary. This extension increases the interval size while preserving the spacing, which causes the grid in momentum space to become denser, $\Delta p \rightarrow \Delta p/2^m$, over the same frequency domain $[-L_p/2, L_p/2]$.

As a corollary, the study of the two-way interpolation schemes and the Nyquist-Shannon theorem provides us with the optimal sampling or discretization for a function, given the domain sizes L_p and L_x in momentum and position space, respectively. Our argument is that for the sampling theorem to succeed and to provide us with good interpolations (10) and (12), the spacings in

momentum and position need to satisfy $\Delta x^{(n)} \leq 2\pi/L_p$ and $\Delta p^{(n)} \leq 2\pi/L_x$. This is achieved with a minimum number of qubits, given by

$$n_{\min} \leq \log_2 \left(\frac{L_p L_x}{2\pi} \right). \quad (14)$$

We use this estimate in our numerical studies and following sections.

2.1.3 Variational quantum algorithm

Now that we have an association between states in a quantum register and the space of bandwidth-limited differentiable functions, we can discuss the Hamiltonian PDE's (1). We associate to the differential operator (2) a quantum representation $\hat{H}^{(n)} = D(\hat{p}^{(n)}) + V(\hat{x}^{(n)})$ where the position and differential operators $V(\hat{x})$ and $D(\hat{p})$ are defined by

$$V(\hat{x}^{(n)}) := \sum_s V(x_s) |s\rangle\langle s|, \quad (15)$$

$$D(\hat{p}^{(n)}) := \hat{\mathcal{F}}^{-1} \sum_s D(p_s) |s\rangle\langle s| \hat{\mathcal{F}}. \quad (16)$$

With this identification, we can translate the search for the stationary solutions (1) to the quest for eigenstates of the \hat{H} operator, using the variational quantum eigensolver [21, 33]. Using a dense variational family of unitary operators $W(\boldsymbol{\theta})$ acting on n qubits, we will define a continuous family of trial states $|f_{\boldsymbol{\theta}}^{(n)}\rangle := W(\boldsymbol{\theta})|0\rangle^{\otimes n}$ and a cost function

$$E(\boldsymbol{\theta}) := \langle f_{\boldsymbol{\theta}}^{(n)} | \hat{H}^{(n)} | f_{\boldsymbol{\theta}}^{(n)} \rangle. \quad (17)$$

In order to approximate the solution to Eq. (1) with minimal eigenvalue E , we will use the continuous function associated to the quantum state $|f_{\boldsymbol{\theta}_{\min}}^{(n)}\rangle$ that results from the variational search

$$\boldsymbol{\theta}_{\min} := \operatorname{argmin} E(\boldsymbol{\theta}). \quad (18)$$

We implement this search as a hybrid algorithm, with a classical algorithm that optimizes $E(\boldsymbol{\theta})$ using the estimations of $E(\boldsymbol{\theta})$ provided by a quantum computer—or a simulator thereof. In the NISQ scenario we do not have access to the exact value of $E(\boldsymbol{\theta})$ but a randomized estimator that results from a finite set M of measurements. In this work we estimate this “energy” as the sum of two random variables, one arising from measurements of the position and another one from the momentum operator

$$E(\boldsymbol{\theta}) \simeq \bar{E}_M := \bar{V}_M + \bar{D}_M + \mathcal{O}\left(\frac{1}{\sqrt{M}}\right). \quad (19)$$

Note that the values of \bar{V}_M and \bar{D}_M are computed separately, creating the quantum states $|f_{\boldsymbol{\theta}}^{(n)}\rangle$ and $|\tilde{f}_{\boldsymbol{\theta}}^{(n)}\rangle := \hat{\mathcal{F}}|f_{\boldsymbol{\theta}}^{(n)}\rangle$ in different experiments, and measuring those states in the computational basis. This approach leads to statistical uncertainties that are of the order $\Delta\hat{V}/\sqrt{M}$ and $\Delta\hat{D}/\sqrt{M}$. Better algorithms could be constructed by using amplitude estimation over approximate implementations of the unitary operator $\exp(-i\hat{H}\Delta t)$, but this requires an infrastructure and a precision of gates that is not presently available.

2.2 Quantum variational circuits

The variational quantum eigensolver (VQE) relies on a parameterized quantum circuit $W(\boldsymbol{\theta})$, that creates the variational ansatz. Many VQE studies use physically motivated structures, such as coupled cluster expansions [21, 34, 35], or random circuits with layers of local unitaries interleaved with layers of entangling operations [36, 37]. In this work we design our variational ansätze $W(\boldsymbol{\theta})$ to approximate the encoding of real discretized functions $|f^{(n)}\rangle$, introducing also new, smoother and less chaotic ansätze.

2.2.1 R_Y ansatz

As baseline for our study, we use a variational ansatz that combines CNOT gates with local, real-valued transformations on the qubits generated by the σ^y operator (c.f. Fig. 3a). The result is a parameterized unitary

$$W(\boldsymbol{\theta}) = \prod_{q=0}^{n-1} R_q^y(\theta_q^{\text{depth}+1}) \times \prod_{d=1}^{\text{depth}} \left[\prod_{c=0}^{n-1} \prod_{t < t} \text{CNOT}_{c,t} \prod_{q=0}^{n-1} R_q^y(\theta_q^d) \right], \quad (20)$$

where the parameters are the angles of the $R_Y(\theta) = \exp(-i\theta\sigma^y/2)$ rotations. This variational ansatz is available in many quantum computing frameworks, including Qiskit [38], which is the one used for our simulations.

2.2.2 Zalka-Grover-Rudolph (ZGR) ansatz

We can derive a better variational ansatz for real functions using the ideas from Zalka [1], and Grover and Rudolph [2], to discretize non-negative probability distributions in a quantum

register. In their work they showed that probability distributions could be approximated by conditional rotations of the least significant qubits based on the state of all previous qubits,

$$|f_{\theta}^{(n)}\rangle = \prod_{i=n-1}^1 \prod_{z_i=0}^{2^{i-1}-1} \exp(i\theta_i(z_i)\sigma_i^y |z\rangle\langle z|) |0\rangle^{\otimes n}. \quad (21)$$

Here, z_i is an integer constructed from the i first qubits, $z = s_0s_1\cdots s_{i-1}$ and $\theta_i(z_i)$ is a collection of angles designed to reproduce the desired function. Note how this is a constructive process where the state of a qubit with low significance i is determined by controlled rotations defined by the more significant qubits $j \in \{0, 1, \dots, i-1\}$.

In practice, the construct from Zalka et al. could be implemented using σ^y rotations and CNOT's. Inspired by this idea, we designed a new variational ansatz (c.f. Fig. 3b) where such rotations are parameterized by a similar number of angles and is slightly more efficient

$$|f_{\theta}^{(n)}\rangle = \prod_{i=n-1}^1 \prod_{z_i=0}^{2^{i-1}-1} e^{i\theta_i z_i \sigma^y} N(z, i) e^{i\theta_{00} \sigma_0^y} |0\rangle^{\otimes n}. \quad (22)$$

The N is a CNOT rotation of the i -th qubit, controlled by a j qubit which is determined by the most significant bit that is active in $(z \text{ xor } (z-1))$. As in the previous construct, the exponentially growing number of parameters makes this an ill-advised choice for very large computations, but we use it because (i) it illustrates the required ordering of conditional operations, from high to low-significant bits, (ii) it is more accurate than the pure R_y ansatz, (iii) it pushes the limits of the variational method and (iv) in practice it gets extremely close to the exact construct, but does not require additional NOT's.

2.2.3 Symmetrization of variational circuits

We can significantly reduce the number of variational parameters by embedding the symmetries of the function in the circuit. Let us consider discretized functions with reflection symmetry, $f(x) = (-1)^\lambda f(-x)$, with $\lambda = \pm 1$. This symmetry can be added to the variational ansatz, engineering first a unitary U_f that describes the function in the positive sector $0 \leq x \leq L_x/2$ with $n-1$ qubits, and applying unitary operations that extend this state to n qubits, covering also the negative part of the discretization $-L_x/2 \leq x \leq L_x/2$.

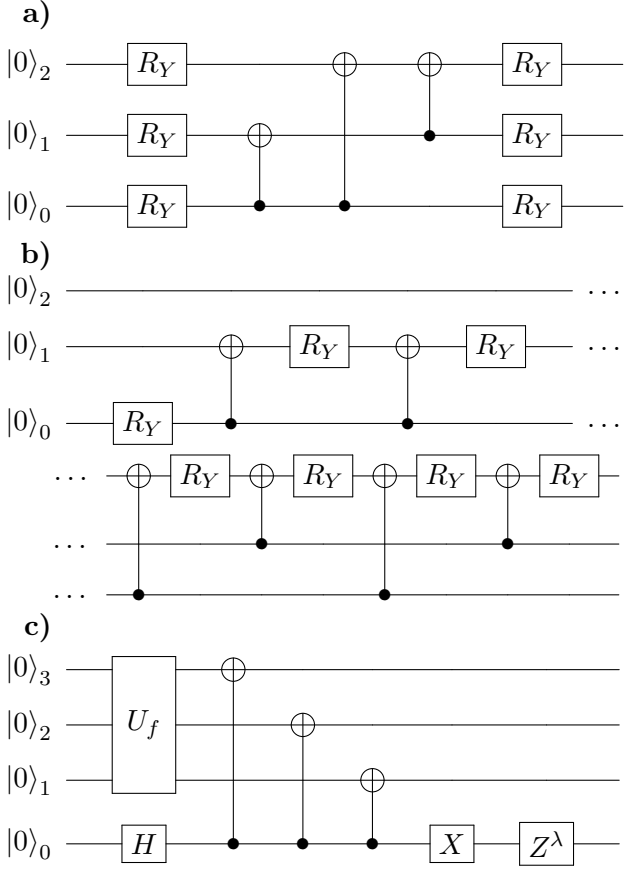


Figure 3: Variational representation of 1D smooth functions. (a) R_Y ansatz of depth one, with full entanglement over three qubits. (b) ZGR ansatz to represent a function $f(x)$ with three qubits. (c) Ansatz to represent a (anti-)symmetric function, $g(x) = (\text{sign } x)^{\text{sym}} f(|x|)$, where U_f encodes $f(x > 0)$.

For this encoding to succeed, we first need to impose a discretization of the space that is also symmetric, which we do by slightly changing the relation between qubit states and positions

$$x_s^{(n)} = -\frac{L_x}{2} + \left(s + \frac{1}{2}\right) \Delta x. \quad (23)$$

With this, our symmetrized function satisfies

$$\langle 1s_1 \dots s_{n-1} | f^\lambda \rangle = (-1)^\lambda \langle 0\bar{s}_1 \dots \bar{s}_{n-1} | f \rangle. \quad (24)$$

Note how positive coordinates $x_s > 0$ relate to the negative ones $x_s < 0$ through the 2's complement relation, which involves negating all bits. These relations can be embedded into the variational circuit as shown in Fig. 3c. First, we create the most significant bit of the wavefunction s_n on a quantum superposition of both $s_0 = 1$ ($x_s > 0$) and $s_0 = 0$ ($x_s < 0$). We then create the

encoded function for the positive valued coordinates in the $n-1$ least significant qubits. Finally, we apply a 2's complement unitary operation to reverse the orientation of the function in the negative coordinates (24) and to set the right sign for the encoded state.

Note that other symmetrization methods can be found in the literature, such as the one in Ref. [39]. This work presents a symmetry-adapted variational quantum eigensolver using a projection operator, whose non-unitarity leads to a classical post-processing. Our approach symmetrizes the state by adding one qubit to the circuit and a small number of single- and two-qubit gates, which is a fully coherent approach and does not require any post-processing.

3 Benchmark equations

We will benchmark our variational quantum PDE solver using two important equations: the quantum harmonic oscillator (25) and the equation for the transmon qubit (28). They both produce simple, highly differentiable functions that can be analytically computed. However, they also involve different boundary conditions, which makes the practical study a bit more interesting.

3.1 Harmonic oscillator

The Schrödinger equation of an harmonic oscillator of mass m and angular frequency ω is

$$\left(-\frac{\hbar^2}{2m}\partial_x^2 + \frac{1}{2}m\omega^2x^2 - E\right)f(x) = 0. \quad (25)$$

The exact solutions to this problem are given by

$$f_n(x) = \left(\frac{\beta^2}{\pi}\right)^{1/4} \frac{1}{\sqrt{2^n n!}} e^{-\beta^2 x^2/2} H_n(\beta x), \quad (26)$$

where $\beta = \sqrt{m\omega/\hbar}$ and H_n is the Hermite polynomial of order n . For $m = \omega = \hbar = 1$, we obtain the ground state of the harmonic oscillator, which is a trivial Gaussian

$$f_0(x) = \frac{1}{\pi^{1/4}} e^{-x^2/2}. \quad (27)$$

This function is real, symmetric and even, and is thus particularly well suited for the variational ansätze discussed above.

In our quantum numerical analysis, we constrain eq. (25) to a finite domain $|x| \leq L_x/2$, defined symmetrically around the origin as in (23). Following the prescriptions from the Nyquist-Shannon theorem, we vary the length of the interval according to the number of available qubits, as $L_x = \sqrt{2\pi 2^n}$, to maximize the accuracy both in position and momentum space.

3.2 Transmon qubit

The eigenstates for a superconducting transmon qubit [40] without charge offset are obtained by solving the equation

$$(4E_C\partial_\varphi^2 - E_J \cos(\varphi) - E) f(\varphi) = 0. \quad (28)$$

The phase variable is periodic over the interval $\varphi \in [-\pi, \pi]$. The model is parameterized by the Josephson energy E_J and the capacitive energy E_C , which we choose $E_C = E_J/50$. The eigenfunctions of the transmon qubit are given by the Mathieu functions, analytical solutions of Mathieu's differential equation

$$\frac{d^2y}{dx^2} + (a - 2q \cos 2x)y = 0. \quad (29)$$

If we expand the problem around $\varphi = 0$, in the limit of large E_J/E_C ,

$$H = 4E_C\partial_\varphi^2 - \frac{1}{2}E_J\varphi^2, \quad (30)$$

which behaves like an harmonic oscillator with

$$\frac{\hbar^2}{2m} \sim 4E_C, \quad \frac{1}{2}E_J \sim \frac{1}{2}m\omega^2, \quad (31)$$

and effective frequency $\hbar\omega = \sqrt{8E_C E_J}$. Therefore, in some regimes the transmon ground state can be approximated by a Gaussian function

$$\psi(\varphi) \propto \exp\left[-\frac{1}{2}\left(\frac{\varphi}{a_0}\right)^2\right], \quad (32)$$

in the dimensionless variable $x = \varphi/a_0$ with unit length

$$a_0^4 = \frac{8E_C}{E_J}. \quad (33)$$

The Gaussian approximation is not perfect, as it fails to capture the nonlinear contributions and does not take into account the periodicity of the function $f(\varphi)$. In particular, unlike the case of the harmonic oscillator, we are not free to choose the interval length, which is fixed to 2π .

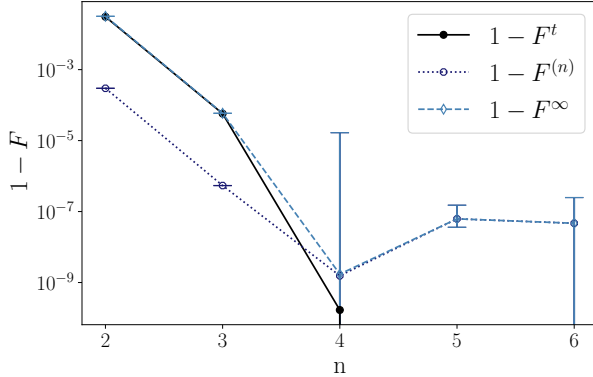


Figure 4: Comparison of the infidelity figures of merit (the median and the standard deviation around the mean of 100 repetitions) for the ZGR ansatz for the numerical limit. The theoretical infidelity $1 - F^t$ is the infidelity of the theoretical 2^n -point wavefunction interpolated up to 2^{12} points and the theoretical 2^{12} -point wavefunction. The n -qubit infidelity $1 - F^{(n)}$ is the infidelity of the n -qubit function obtained from the optimization and the 2^n -point theoretical function. The continuous infidelity $1 - F^\infty$ is the infidelity of the n -qubit function interpolated up to 2^{12} points and the 2^{12} -point theoretical function

4 Numerical results

In this section we study the application of our variational quantum PDE solver to the harmonic oscillator and the transmon qubit. We use the ZGR and the R_Y variational ansätze, searching the ground state solution and energy for 2, 3, 4, 5 and 6 qubits. The first part of this study combines an idealized quantum computer simulated by Qiskit [38], with three classical optimizers: COBYLA, a gradient free method, SPSA, an stochastic optimizer with numerical gradient, and ADAM, which we combine with an analytic estimate of the gradient [41, 42]. In the last part of this section we discuss how the algorithm performs in a more realistic scenario with errors, analyzing how these errors affect both the evaluation of the function and its properties.

4.1 Figures of merit

When solving the PDE's we can compare the performance of the algorithms using different metrics, such as time, number of evaluations of the cost function, precision in the evaluation of the energy and precision in the determination of the encoded function. We focus on the last two.

To analyze the quality of the variational state at the end of the simulation we use the fidelity $F[\psi_1, \psi_2] := |\langle \psi_1 | \psi_2 \rangle|^2$. We may compute the fidelity between the variational states produced by the optimization $W(\boldsymbol{\theta}_{\text{opt}}) |0\rangle$, with the discretized function using the same number of qubits $|f^{(n)}\rangle$

$$F^{(n)} := \left| \langle f^{(n)} | W(\boldsymbol{\theta}_{\text{opt}}) | 0^{\otimes n} \rangle \right|^2. \quad (34)$$

This first figure of merit may be arbitrarily small, but it does not characterize how much information we have about the continuous function that is the solution to our problem $f(x)$. To fully understand this we need to gauge the quality of the continuous function that we associate to the quantum register (10). This gives us a different figure of merit, which we call the *continuous fidelity*, which is obtained by using the quantum Fourier interpolation algorithm (11)

$$F^\infty := \lim_{m \rightarrow \infty} \left| \langle f^{(n+m)} | U_{\text{int}}^{n,m} W(\boldsymbol{\theta}_{\text{opt}}) | 0^{\otimes n} \rangle \right|^2. \quad (35)$$

In Fig. 4 we compare the infidelities $1 - F^{(n)}$ and $1 - F^\infty$ obtained with the ZGR ansatz and the best optimization method. We also show, for comparison, the best numerical approximation (10) that we can obtain using a finite grid with 2^n points. Note how the errors in the quantum state overestimate our true knowledge of the function $F^{(n)} \geq F^\infty$. Consequently, in our later plots we will represent the median of the infidelities $1 - F^\infty$ over 100 repetitions of each simulation with different initial states or trajectories, and the error bars will be the standard deviation around the mean. Moreover, we estimate F^∞ using $m = 12 - n$ extra qubits, which already gives a good converged measure.

In addition to the quantum state, we are also interested in how well we can estimate the properties of the solution to the PDE. We gauge this by evaluating the relative error in the computation of the energy

$$\varepsilon = \left| \frac{E_{t_n} - E_{\text{opt}}}{E_1 - E_0} \right|. \quad (36)$$

This is a dimensionless figure of merit that is adapted to the natural energy scales of the problem: E_{t_n} is the theoretical energy obtained over a grid with 2^n points, E_{opt} is the optimal energy derived by the algorithm, and $E_1 - E_0$ is the energy

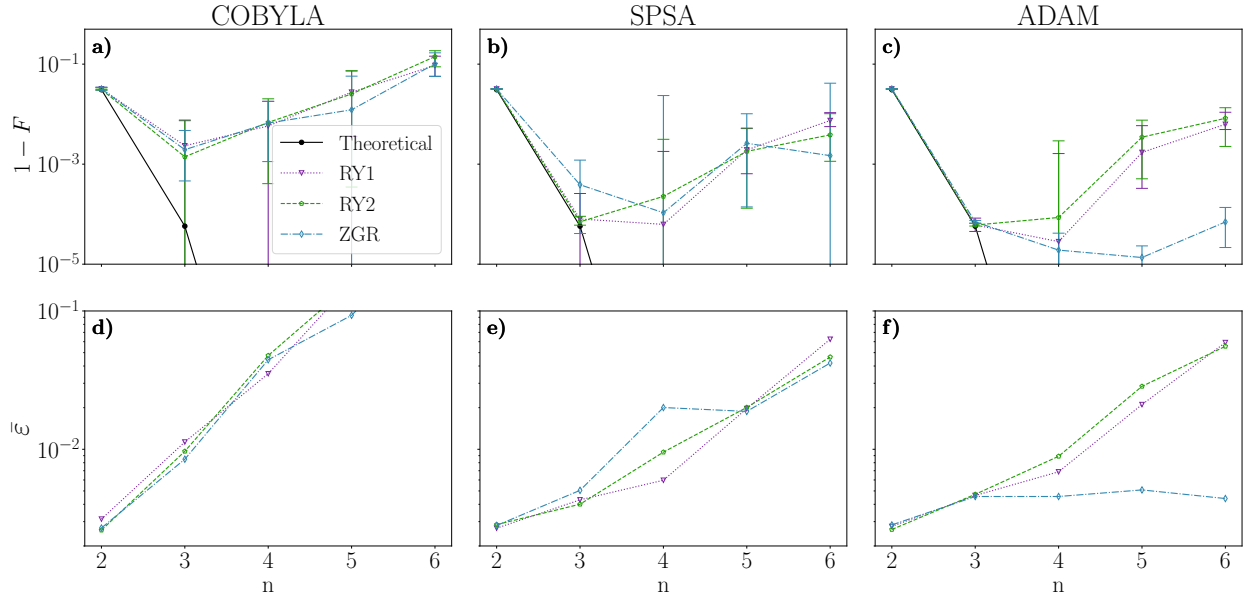


Figure 5: Results of the simulations for 2, 3, 4, 5 and 6 qubits with 8192 evaluations for the harmonic oscillator using the ZGR and the R_Y ansätze with depth 1 (RY1) and 2 (RY2) and the COBYLA, SPSA and ADAM optimizers. (a) Continuous infidelity with $n + m = 12$. (b) Rescaled energy $\bar{\varepsilon}$ (36).

difference between the lowest and first excited solutions of the PDE (1). In idealized applications we expect ε and $1 - F^\infty$ to be proportional to each other, but this is not always true in real-world quantum computers, as we see below.

4.2 Harmonic oscillator

We applied the variational quantum PDE solver to the harmonic oscillator model from section 3.1. The actual results are summarized in Table 1 and on Figure 5. On the first row of these plots, Figures 5a-c show the infidelity $1 - F^\infty$ of the optimal state, as obtained with three different optimizers and three versions of the variational ansatz. As reference, we also plot the lowest infidelity obtained with the best approximation (10) on the same grid. Figures 5d-e illustrate the relative error in the prediction of the energy (36) for the same optimal states.

From these figures we conclude that the best optimization method is ADAM, followed closely by the SPSA. Both methods seem to excel due to their tolerance to the intrinsic uncertainty in the estimation of the energy. However, while ADAM uses an analytic estimate of the cost-function's gradient [41, 42], SPSA relies on a stochastic estimate with errors that get amplified by small denominators. Thus, even for the same ansatz,

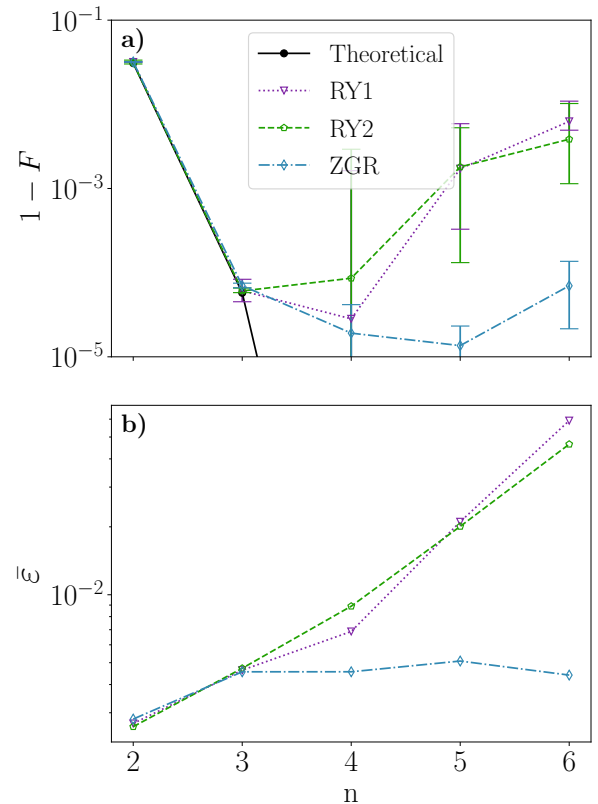


Figure 6: Lowest infidelity results for the simulations for 2, 3, 4, 5 and 6 qubits with 8192 evaluations for the harmonic oscillator using the ZGR and the R_Y ansätze with depth 1 (RY1) and 2 (RY2). (a) Continuous infidelity $\bar{\varepsilon}$ (36).

SPSA leads to worse estimates of the function and of the optimal energy.

From Fig. 6 one may conclude that ZGR is the best variational ansatz for this problem; however, one should wonder how much of the difference can be attributed to the ansatz and how much to the optimizer. To ease this comparison, Table 1 shows the average infidelities from four methods, including simulations with the L-BFGS-B optimizer and an infinite number of measurements¹. This table shows that neither the R_Y ansatz nor the ZGR achieve the best possible fidelity. However, the former gets trapped in local minima and loses fidelity by 1 to 3 orders of magnitude as we use more than 3 qubits.

We attribute the difference in precision to the fact that the ZGR ansatz is designed for the representation of continuous functions [1, 2]. In this ansatz, every rotation builds on the previous ones in a smooth, easily differentiable fashion, without any loss of information. In the R_Y , however, the influence of different qubits and layers is more inefficiently transported by the layers of entangling unitaries, leading to the vanishing of gradients [43]. This chaotic nature is more manifest as we increase the number of qubits and parameters to optimize.

In any case, one should emphasize that the infidelities that we obtain, in the range 10^{-5} to 10^{-3} , lay well below what is expected from the statistical uncertainty with which we evaluate the cost function. To illustrate this, Figure 7b shows one of the stochastic trajectories created by the ADAM method for the ZGR ansatz. In dashed line we plot the evaluation of the cost function as returned by the simulator $\bar{E}_M(\theta)$, surrounded by a colored band that estimates the statistical uncertainty for $M = 8192$ measurements. This trajectory and error band must be compared to the actual energy computed for the same parameters $E(\theta_i)$, without any uncertainty. This quantity approaches a relative error $\varepsilon \simeq 5 \times 10^{-3}$, which is two orders of magnitude below the statistical uncertainty, illustrating the power of stochastic optimization.

In Figure 7a we can observe how with just 3-qubits we recover the theoretical wavefunction

¹In other words, we extract the full expectation value from the wavefunction, without any statistical errors, and use an optimizer that works extremely well in this scenario.

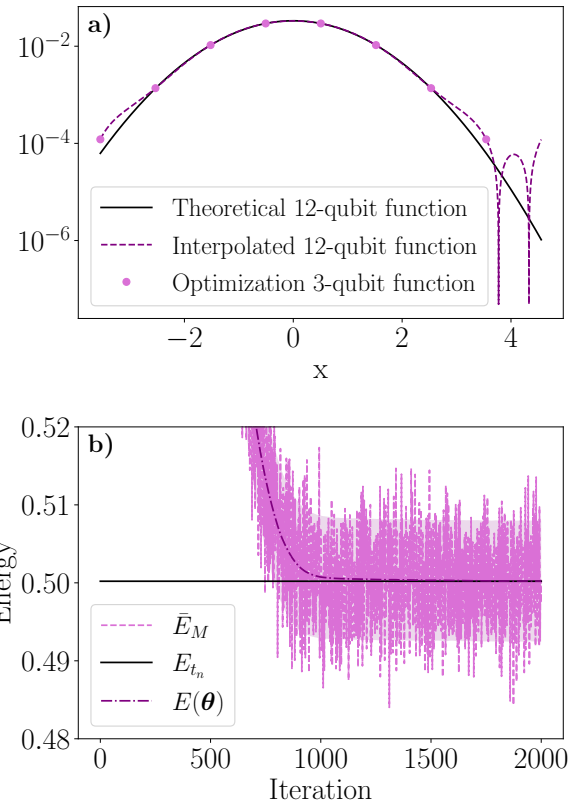


Figure 7: Result for the optimization for the ADAM optimizer and the ZGR ansatz for 3 qubits. a) Absolute value of the theoretical and optimization wavefunctions. b) Value of the energy for each iteration.

with high fidelity using interpolation, as most of the information is obtained from the original points as the fidelity points to. The behaviour of the interpolation for greater x values is a result of discontinuities in the interval of interpolation when using the Fourier transform.

The precision of the algorithm is limited by the number of evaluations in the quantum computer, as the more evaluations the better the estimate of the expectation value. Figure 8b shows this behaviour: by increasing the number of evaluations by a factor 4, we decrease the value of the error in the energy ε by a factor 2. This improvement in the energy leads to an increase of the fidelity (see Fig. 8a).

4.3 Transmon qubit

The results of the transmon qubit simulations are shown in Figs. 9a-f. These plots confirm the observations made for the harmonic oscillator. Once more, the ADAM optimizer leads to the lowest

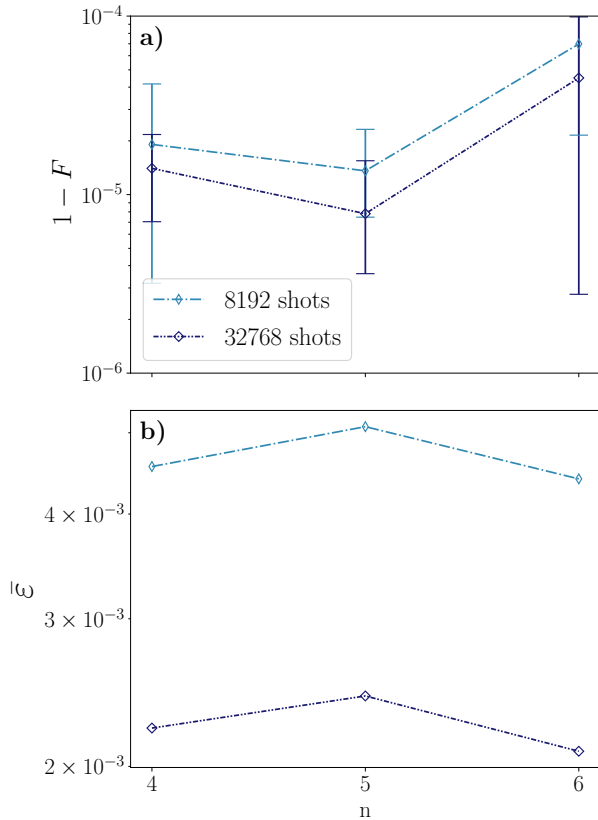


Figure 8: Result for the optimization for the ADAM optimizer and the ZGR ansatz for 8192 and 32768 evaluations. (a) Continuous infidelity with $n + m = 12$. (b) Rescaled energy $\bar{\epsilon}$ (36).

infidelity results, due to the use of the analytic gradient. The ZGR ansatz also behaves better than the R_Y , and no ansatz achieves the minimum infidelity that can be reached with 3 – 6 qubits, probably for the same reasons as before: local trapping and statistical uncertainty.

When we compare the harmonic oscillator and the transmon, we see that the latter is typically affected by greater infidelities. The zeroth order solution of the Mathieu equation (29), which is the transmon ground state, is more complicated to reproduce than the Gaussian function of the ground state of the harmonic oscillator (27). First, this is a periodic function that does not strictly vanish on the boundaries. Second, contrary to the Gaussian function, we are not allowed to change the length of the interval to maximize the precision in both position and momentum space. All together, as shown in Table 2, the achievable infidelities are strictly worse for all ansätze, even when using numerical exact optimizations (L-BFGS-B).

We chose the transmon qubit equation because it is a physically motivated problem. One might wonder about the utility of this method for the computation of actual properties, such as the energies and excitation probabilities of actual qubits. The relative errors that we have obtained, $10^{-3} – 10^{-2}$ are compatible to what can be expected from using 8192 shots. One could further decrease to the theoretical limits, using more measurements. However, in order to achieve a relative error below 10^{-4} (a fraction of a MHz), one would need to use about 100 to 10,000 times more measurements in the final stages of the optimization. While this seems doable, it suggests the need to find better strategies for the energy evaluation or even the optimization itself.

4.4 Application to NISQ devices

Until now we have focused on the performance of our algorithm under ideal circumstances. However, the actual motivation of variational methods is to work in NISQ devices, where qubits have finite lifetimes and gates are imperfect, but even imperfect variational constructs can be optimized to approach the ideal limits [22]. In a similar spirit, we will now evaluate the noise tolerance of the variational quantum PDE solver, to understand its suitability for existing and near-term quantum computers.

Our study is performed using a simulator of the `ibmq_santiago` 5-qubit ² [38] quantum computer. This simulator allows us to store the noise model, coupling map and basis gates, so that each computation is subject to identical conditions. The noise model includes the gate error probability and gate length for each basis gate and qubit, and the readout error probabilities and T_1 and T_2 relaxation times for each qubit. For this device, T_1 and T_2 are of the order of $100 \mu s$, and the readout probability is $\sim 10^{-2}$. The gate error for single-qubit gates is of order $10^{-4} – 10^{-3}$ with gate length of order $10 ns$, while both the gate error and length are one order of magnitude greater for two-qubit gates ³.

Our study applies the R_Y ansatz with depth 1 to the solution of the harmonic oscillator, using the SPSA optimizer. We chose the ansatz

²<https://quantum-computing.ibm.com/>

³The results are for the `ibmq_santiago` calibration with date 17/03/2021.

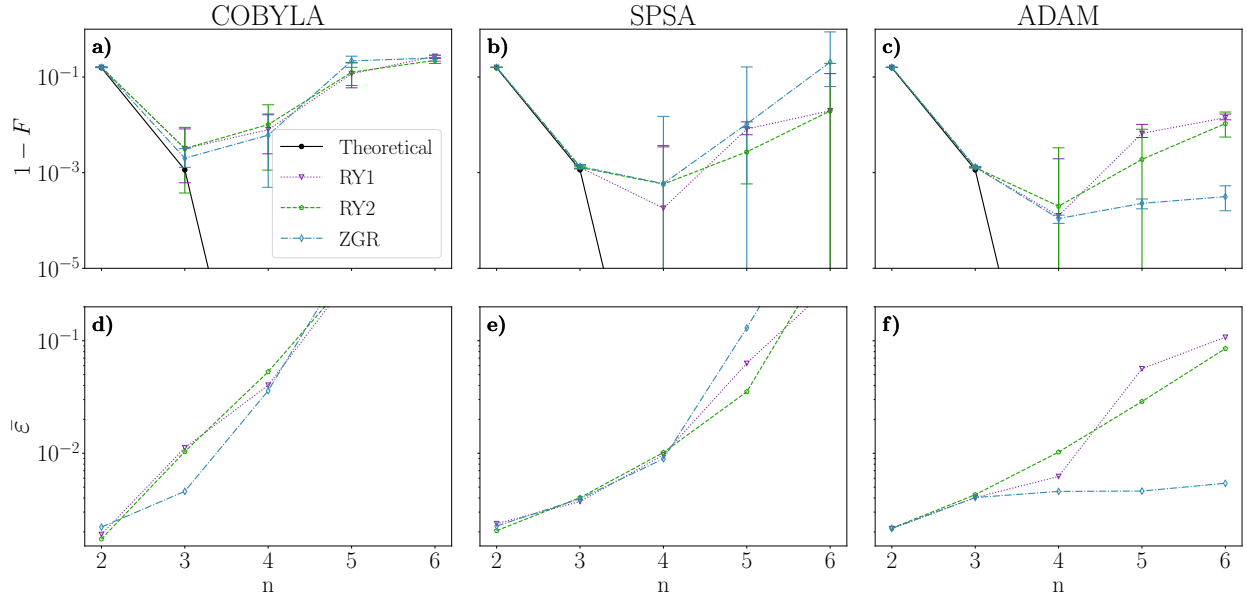


Figure 9: Results of the simulations for 2, 3, 4, 5 and 6 qubits with 8192 evaluations for the transmon qubit using the ZGR and the R_Y ansätze with depth 1 (RY1) and 2 (RY2) and the COBYLA, SPSA and ADAM optimizers. (a) Continuous infidelity with $n + m = 12$. (b) Rescaled energy $\bar{\varepsilon}$ (36).

and problem that provide the best fidelities, with the least number of gates, combined with an optimizer that is expected to perform well in noisy problems. Figure 10a shows the infidelity of the continuous function in the ideal and noisy simulations. The fidelity decreases with the number of qubits due to the greater number of gates, which introduce more errors and increase the effect of decoherence due to the longer time of the circuit. However, for a small number of qubits, it is possible to obtain a reasonably small error of 10^{-3} for 3-qubits, which allows us to reconstruct the theoretical continuous wavefunction.

Although the optimization of the parameters is successful, we obtain a very significant error in the evaluation of the energy (Fig. 10b), even for a small number of qubits. We attribute this error to the circuits that we use to evaluate the energy in position and momentum space. We can confirm this hypothesis using Qiskit's quantum tomography toolbox for a small number of qubits, using the `ibmq_santiago` simulator. As shown in Figure 11, the errors in the two circuits can be quite significant, and are larger in momentum space because of the gates that are required for the QFT.

Despite the errors in these circuits, the fact that we obtain a good quality estimate of the function itself suggests that we can apply er-

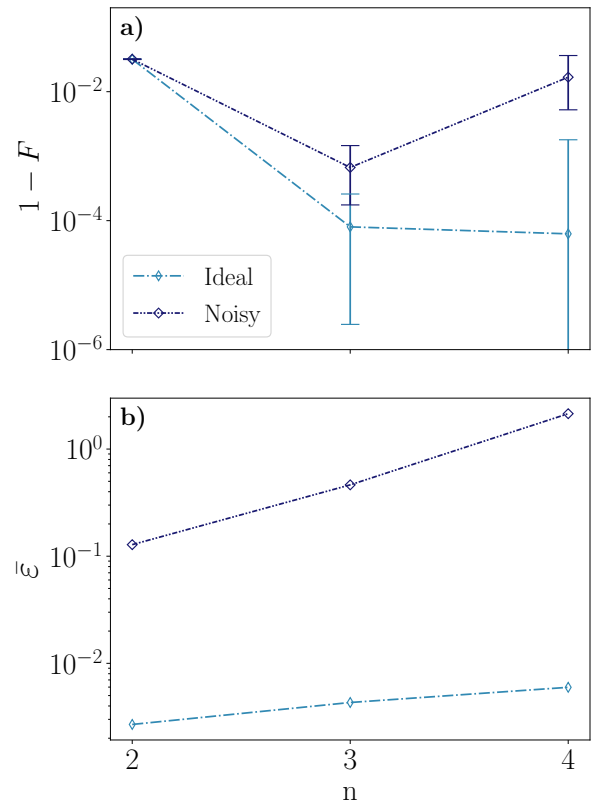


Figure 10: Results for the ideal and noisy (ibmq_santiago noise model) optimization for the SPSA optimizer and the RY1 ansatz with 8192 evaluations for the harmonic oscillator. (a) Continuous infidelity with $n + m = 12$. (b) Rescaled energy $\bar{\varepsilon}$ (36).

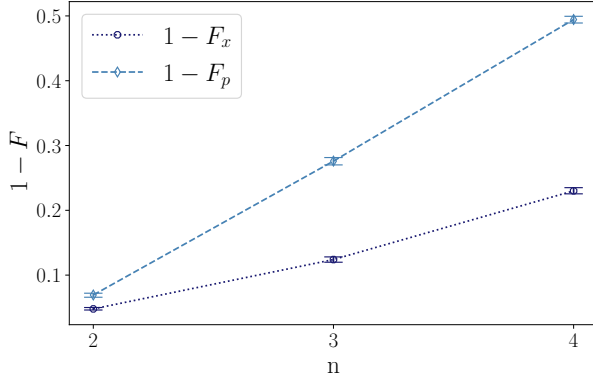


Figure 11: Circuit infidelity for the position $1 - F_x$ and momentum $1 - F_p$ circuits for the RY1 ansatz with 8192 evaluations for 100 simulations and the `ibmq_santiago` noise model.

rror mitigation and zero-noise extrapolation [44]. To test this hypothesis, we repeat the simulations using a simpler noise model dominated by thermal relaxation, where we can tune T_1 , but still use the coupling map and basis gates of the `ibmq_santiago` 5-qubit device. In this study we prepare a quantum circuit with the optimal solution for 3 qubits and estimate the energy using 819200 evaluations, for different values of T_1 . As figure 12 shows, if $T_1 \geq 5\mu\text{s}$, the energy admits a Taylor expansion of 6-th order

$$E(T_1) = E_0 + \sum_n \epsilon_n \frac{1}{T_1^n}. \quad (37)$$

This expansion can be used by itself or with Richardson extrapolation [44] to estimate values of the energy with a lower error, of order $\varepsilon \sim 10^{-2}$ for values of $T_1 \sim 100 - 50 \mu\text{s}$, which are within the experimental range. Therefore, we can conclude that the thermal relaxation time limits the energy estimation but it is possible to recover the theoretical value with absolute error of the order of 10^{-2} with results with thermal relaxation times characteristic of state of the art devices.

5 Conclusions and future perspectives

We have developed a variational quantum algorithm to solve Hamiltonian PDE's. The algorithm makes use of quantum interpolation to derive an efficient representation of continuous functions in quantum registers. We combine this algorithm with newer variational ansätze that are

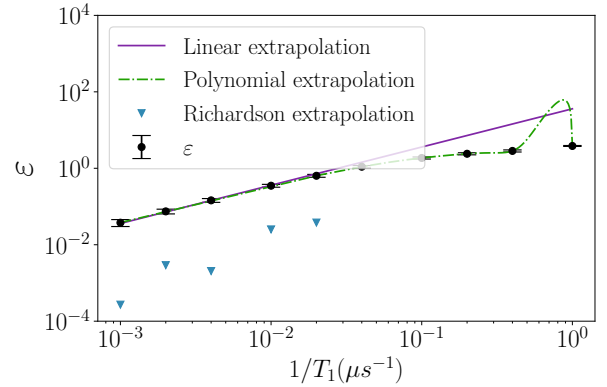


Figure 12: Energy results for the harmonic oscillator energy evaluation with thermal relaxation noise for the RY1 ansatz for 3 qubits.

better suited to describe continuous differential functions, or which include symmetries. We have tested these ideas in idealized scenarios with infinite or limited number of measurements, obtaining excellent accuracy— 10^{-5} infidelity—even with small numbers of qubits. In addition, under the presence of noise sources the algorithm is still efficient, reaching high fidelity results— $10^{-3} - 10^{-4}$ infidelity—for 3 qubits.

The good results obtained for the ZGR ansatz point to the possibility to develop simplified ansätze to represent quantum states with a lower growth of the dimensions of the parameter space, but with a similar philosophy to construct the quantum states. Moreover, less demanding gradient computing techniques can also be implemented [45] and it is also possible to extend this method to solve PDE's in higher dimensional spaces.

However, as in all variational methods, we have seen that the accuracy is ultimately limited by our statistical uncertainty in the determination of the cost function and the analytic gradients. Assume for instance that we want to use the present method to study a transmon qubit. Reaching the required experimental precision, with errors $\varepsilon \simeq 10^{-4}$ can be costly in a scenario of NISQ computers with limited access and temporal stability. It also requires significant improvements in both the classical optimization and the quantum evaluation of properties. In such a scenario, it may be worth considering alternative quantum-inspired methods that can benefit from similar encodings, and also provide heuristic advantages for the same type of equations [30].

This work has been supported by FPU Grant FPU19/03590, Spanish project PGC2018-094792-B-I00 (MCIU/AEI/FEDER, UE), CAM/FEDER project No. S2018/TCS-4342 (QUITEMAD-CM) and CSIC Quantum Technology Platform PT-001.

References

- [1] Christof Zalka. Simulating quantum systems on a quantum computer. *Proceedings of the Royal Society of London. Series A: Mathematical, Physical and Engineering Sciences*, 454(1969):313–322, jan 1998. [DOI: 10.1098/rspa.1998.0162](https://doi.org/10.1098/rspa.1998.0162).
- [2] Lov Grover and Terry Rudolph. Creating superpositions that correspond to efficiently integrable probability distributions. *arXiv e-prints*, art. [quant-ph/0208112](https://arxiv.org/abs/quant-ph/0208112), August 2002.
- [3] Bolesław Kacewicz. Almost optimal solution of initial-value problems by randomized and quantum algorithms. *Journal of Complexity*, 22(5):676–690, oct 2006. [DOI: 10.1016/j.jco.2006.03.001](https://doi.org/10.1016/j.jco.2006.03.001).
- [4] Sarah K. Leyton and Tobias J. Osborne. A quantum algorithm to solve nonlinear differential equations. *arXiv e-prints*, art. [arXiv:0812.4423](https://arxiv.org/abs/0812.4423), December 2008.
- [5] Frank Gaitan. Finding flows of a navier–stokes fluid through quantum computing. *npj Quantum Information*, 6(1), jul 2020. [DOI: 10.1038/s41534-020-00291-0](https://doi.org/10.1038/s41534-020-00291-0).
- [6] Dominic W Berry. High-order quantum algorithm for solving linear differential equations. *Journal of Physics A: Mathematical and Theoretical*, 47(10):105301, feb 2014. [DOI: 10.1088/1751-8113/47/10/105301](https://doi.org/10.1088/1751-8113/47/10/105301).
- [7] Aram W. Harrow, Avinatan Hassidim, and Seth Lloyd. Quantum algorithm for linear systems of equations. *Physical Review Letters*, 103(15), oct 2009. [DOI: 10.1103/physrevlett.103.150502](https://doi.org/10.1103/physrevlett.103.150502).
- [8] Dominic W. Berry, Andrew M. Childs, Aaron Ostrander, and Guoming Wang. Quantum algorithm for linear differential equations with exponentially improved dependence on precision. *Communications in Mathematical Physics*, 356(3):1057–1081, oct 2017. [DOI: 10.1007/s00220-017-3002-y](https://doi.org/10.1007/s00220-017-3002-y).
- [9] Andrew M. Childs, Jin-Peng Liu, and Aaron Ostrander. High-precision quantum algorithms for partial differential equations. *arXiv e-prints*, art. [arXiv:2002.07868](https://arxiv.org/abs/2002.07868), February 2020.
- [10] Ashley Montanaro and Sam Pallister. Quantum algorithms and the finite element method. *Physical Review A*, 93(3), mar 2016. [DOI: 10.1103/physreva.93.032324](https://doi.org/10.1103/physreva.93.032324).
- [11] Andrew M. Childs and Jin-Peng Liu. Quantum spectral methods for differential equations. *Communications in Mathematical Physics*, 375(2):1427–1457, feb 2020. [DOI: 10.1007/s00220-020-03699-z](https://doi.org/10.1007/s00220-020-03699-z).
- [12] Yudong Cao, Anargyros Papageorgiou, Iasonas Petras, Joseph Traub, and Sabre Kais. Quantum algorithm and circuit design solving the poisson equation. *New Journal of Physics*, 15(1):013021, jan 2013. [DOI: 10.1088/1367-2630/15/1/013021](https://doi.org/10.1088/1367-2630/15/1/013021).
- [13] Noah Linden, Ashley Montanaro, and Changpeng Shao. Quantum vs. classical algorithms for solving the heat equation. *arXiv e-prints*, art. [arXiv:2004.06516](https://arxiv.org/abs/2004.06516), April 2020.
- [14] Pedro C. S. Costa, Stephen Jordan, and Aaron Ostrander. Quantum algorithm for simulating the wave equation. *Physical Review A*, 99(1), jan 2019. [DOI: 10.1103/physreva.99.012323](https://doi.org/10.1103/physreva.99.012323).
- [15] Adrien Suau, Gabriel Staffelbach, and Henri Calandra. Practical quantum computing: Solving the wave equation using a quantum approach. *ACM Transactions on Quantum Computing*, 2(1):1–35, feb 2021. [DOI: 10.1145/3430030](https://doi.org/10.1145/3430030).
- [16] Jin-Peng Liu, Herman Øie Kolden, Hari K. Krovi, Nuno F. Loureiro, Konstantina Trivisa, and Andrew M. Childs. Efficient quantum algorithm for dissipative nonlinear differential equations. *arXiv e-prints*, art. [arXiv:2011.03185](https://arxiv.org/abs/2011.03185), November 2020.
- [17] Seth Lloyd, Giacomo De Palma, Can Gokler, Bobak Kiani, Zi-Wen Liu, Milad Marvian, Felix Tennie, and Tim Palmer. Quantum algorithm for nonlinear differential equations. *arXiv e-prints*, art. [arXiv:2011.06571](https://arxiv.org/abs/2011.06571), November 2020.
- [18] Tao Xin, Shijie Wei, Jianlian Cui, Junxiang Xiao, Iñigo Arrazola, Lucas Lamata, Xiangyu Kong, Dawei Lu, Enrique Solano, and Guilu Long. Quantum algorithm for solving linear differential equations: Theory and ex-

- periment. *Physical Review A*, 101(3), mar 2020. DOI: [10.1103/physreva.101.032307](https://doi.org/10.1103/physreva.101.032307).
- [19] Juan Miguel Arrazola, Timjan Kalajdzievski, Christian Weedbrook, and Seth Lloyd. Quantum algorithm for nonhomogeneous linear partial differential equations. *Physical Review A*, 100(3), sep 2019. DOI: [10.1103/physreva.100.032306](https://doi.org/10.1103/physreva.100.032306).
- [20] John Preskill. Quantum computing in the NISQ era and beyond. *Quantum*, 2:79, aug 2018. DOI: [10.22331/q-2018-08-06-79](https://doi.org/10.22331/q-2018-08-06-79).
- [21] Jarrod R McClean, Jonathan Romero, Ryan Babbush, and Alán Aspuru-Guzik. The theory of variational hybrid quantum-classical algorithms. *New Journal of Physics*, 18 (2):023023, feb 2016. DOI: [10.1088/1367-2630/18/2/023023](https://doi.org/10.1088/1367-2630/18/2/023023).
- [22] Kunal Sharma, Sumeet Khatri, M Cerezo, and Patrick J Coles. Noise resilience of variational quantum compiling. *New Journal of Physics*, 22(4):043006, apr 2020. DOI: [10.1088/1367-2630/ab784c](https://doi.org/10.1088/1367-2630/ab784c).
- [23] Michael Lubasch, Jaewoo Joo, Pierre Moinier, Martin Kiffner, and Dieter Jaksch. Variational quantum algorithms for nonlinear problems. *Physical Review A*, 101(1), jan 2020. DOI: [10.1103/PhysRevA.101.010301](https://doi.org/10.1103/PhysRevA.101.010301).
- [24] Sam McArdle, Tyson Jones, Suguru Endo, Ying Li, Simon C. Benjamin, and Xiao Yuan. Variational ansatz-based quantum simulation of imaginary time evolution. *npj Quantum Information*, 5(1), sep 2019. DOI: [10.1038/s41534-019-0187-2](https://doi.org/10.1038/s41534-019-0187-2).
- [25] Oleksandr Kyriienko, Annie E. Paine, and Vincent E. Elfving. Solving nonlinear differential equations with differentiable quantum circuits. *arXiv e-prints*, art. [arXiv:2011.10395](https://arxiv.org/abs/2011.10395), November 2020.
- [26] Martin Knudsen and Christian B. Mendl. Solving Differential Equations via Continuous-Variable Quantum Computers. *arXiv e-prints*, art. [arXiv:2012.12220](https://arxiv.org/abs/2012.12220), December 2020.
- [27] Hailing Liu, Yusen Wu, Linchun Wan, Shijie Pan, Sujuan Qin, Fei Gao, and Qiaoyan Wen. Variational Quantum algorithm for Poisson equation. *arXiv e-prints*, art. [arXiv:2012.07014](https://arxiv.org/abs/2012.07014), December 2020.
- [28] Jing-Ning Zhang, Iñigo Arrazola, Jorge Casanova, Lucas Lamata, Kihwan Kim, and Enrique Solano. Probabilistic eigen-
solver with a trapped-ion quantum processor. *Physical Review A*, 101(5), may 2020. DOI: [10.1103/physreva.101.052333](https://doi.org/10.1103/physreva.101.052333).
- [29] Filipe Fontanella, Antoine Jacquier, and Muguad Oumgari. A Quantum algorithm for linear PDE's arising in Finance. *arXiv e-prints*, art. [arXiv:1912.02753](https://arxiv.org/abs/1912.02753), December 2019.
- [30] Juan José García-Ripoll. Quantum-inspired algorithms for multivariate analysis: from interpolation to partial differential equations. *arXiv e-prints*, art. [arXiv:1909.06619](https://arxiv.org/abs/1909.06619), September 2019.
- [31] H. Nyquist. Certain topics in telegraph transmission theory. *Transactions of the American Institute of Electrical Engineers*, 47(2):617–644, apr 1928. DOI: [10.1109/t-aiee.1928.5055024](https://doi.org/10.1109/t-aiee.1928.5055024).
- [32] C.E. Shannon. Communication in the presence of noise. *Proceedings of the IRE*, 37(1):10–21, jan 1949. DOI: [10.1109/jrproc.1949.232969](https://doi.org/10.1109/jrproc.1949.232969).
- [33] Alberto Peruzzo, Jarrod McClean, Peter Shadbolt, Man-Hong Yung, Xiao-Qi Zhou, Peter J. Love, Alán Aspuru-Guzik, and Jeremy L. O’Brien. A variational eigenvalue solver on a photonic quantum processor. *Nature Communications*, 5(1), jul 2014. DOI: [10.1038/ncomms5213](https://doi.org/10.1038/ncomms5213).
- [34] P. J. J. O’Malley, R. Babbush, I. D. Kivlichan, J. Romero, J. R. McClean, R. Barends, J. Kelly, P. Roushan, A. Tranter, N. Ding, B. Campbell, Y. Chen, Z. Chen, B. Chiaro, A. Dunsworth, A. G. Fowler, E. Jeffrey, E. Lucero, A. Megrant, J. Y. Mutus, M. Neeley, C. Neill, C. Quintana, D. Sank, A. Vainsencher, J. Wenner, T. C. White, P. V. Coveney, P. J. Love, H. Neven, A. Aspuru-Guzik, and J. M. Martinis. Scalable quantum simulation of molecular energies. *Phys. Rev. X*, 6:031007, Jul 2016. DOI: [10.1103/PhysRevX.6.031007](https://doi.org/10.1103/PhysRevX.6.031007).
- [35] Cornelius Hempel, Christine Maier, Jonathan Romero, Jarrod McClean, Thomas Monz, Heng Shen, Petar Jurcevic, Ben P. Lanyon, Peter Love, Ryan Babbush, Alán Aspuru-Guzik, Rainer Blatt, and Christian F. Roos. Quantum chemistry calculations on a trapped-ion quantum simulator. *Physical Review X*, 8(3), jul 2018. DOI: [10.1103/physrevx.8.031022](https://doi.org/10.1103/physrevx.8.031022).
- [36] Abhinav Kandala, Antonio Mezzacapo,

- Kristan Temme, Maika Takita, Markus Brink, Jerry M. Chow, and Jay M. Gambetta. Hardware-efficient variational quantum eigensolver for small molecules and quantum magnets. *Nature*, 549(7671):242–246, sep 2017. DOI: [10.1038/nature23879](https://doi.org/10.1038/nature23879).
- [37] Abhinav Kandala, Kristan Temme, Antonio D. Córcoles, Antonio Mezzacapo, Jerry M. Chow, and Jay M. Gambetta. Error mitigation extends the computational reach of a noisy quantum processor. *Nature*, 567(7749):491–495, mar 2019. DOI: [10.1038/s41586-019-1040-7](https://doi.org/10.1038/s41586-019-1040-7).
- [38] Héctor Abraham, AduOffei, Rochisha Agarwal, Ismail Yunus Akhalwaya, and Gadi Aleksandrowicz et al. Qiskit: An open-source framework for quantum computing, 2019.
- [39] Kazuhiro Seki, Tomonori Shirakawa, and Seiji Yunoki. Symmetry-adapted variational quantum eigensolver. *Physical Review A*, 101(5), may 2020. DOI: [10.1103/physreva.101.052340](https://doi.org/10.1103/physreva.101.052340).
- [40] Jens Koch, Terri M. Yu, Jay Gambetta, A. A. Houck, D. I. Schuster, J. Majer, Alexandre Blais, M. H. Devoret, S. M. Girvin, and R. J. Schoelkopf. Charge-insensitive qubit design derived from the cooper pair box. *Physical Review A*, 76(4), oct 2007. DOI: [10.1103/physreva.76.042319](https://doi.org/10.1103/physreva.76.042319).
- [41] K. Mitarai, M. Negoro, M. Kitagawa, and K. Fujii. Quantum circuit learning. *Physical Review A*, 98(3), sep 2018. DOI: [10.1103/physreva.98.032309](https://doi.org/10.1103/physreva.98.032309).
- [42] Maria Schuld, Ville Bergholm, Christian Gogolin, Josh Izaac, and Nathan Killoran. Evaluating analytic gradients on quantum hardware. *Physical Review A*, 99(3), mar 2019. DOI: [10.1103/PhysRevA.99.032331](https://doi.org/10.1103/PhysRevA.99.032331).
- [43] Jarrod R. McClean, Sergio Boixo, Vadim N. Smelyanskiy, Ryan Babbush, and Hartmut Neven. Barren plateaus in quantum neural network training landscapes. *Nature Communications*, 9(1), nov 2018. DOI: [10.1038/s41467-018-07090-4](https://doi.org/10.1038/s41467-018-07090-4).
- [44] Abhinav Kandala, Kristan Temme, Antonio D. Córcoles, Antonio Mezzacapo, Jerry M. Chow, and Jay M. Gambetta. Error mitigation extends the computational reach of a noisy quantum processor. *Nature*, 567(7749):491–495, mar 2019. DOI: [10.1038/s41586-019-1040-7](https://doi.org/10.1038/s41586-019-1040-7).
- [45] Ryan Sweke, Frederik Wilde, Johannes Meyer, Maria Schuld, Paul K. Faehrmann, Barthélémy Meynard-Piganeau, and Jens Eisert. Stochastic gradient descent for hybrid quantum-classical optimization. *Quantum*, 4:314, aug 2020. DOI: [10.22331/q-2020-08-31-314](https://doi.org/10.22331/q-2020-08-31-314).

A Numerical results

# qubits	Ansatz	# parameters	# CNOT's	$1 - F^\infty$ COBYLA	$1 - F^\infty$ SPSA	$1 - F^\infty$ ADAM	$1 - F^\infty$ L-BFGS-B
2	RY1	2	1	0.0320(7)	0.03182(7)	0.03185(4)	$3.19 \cdot 10^{-2}$
	RY2	3	1	0.0310(8)	0.03184(3)	0.03185(0)	$3.19 \cdot 10^{-2}$
	ZGR	1	1	0.0319(7)	0.03186(8)	0.03188(0)	$3.19 \cdot 10^{-2}$
3	RY1	4	3	0.002(3)	0.00008(0)	0.000060(8)	$5.89 \cdot 10^{-5}$
	RY2	6	4	0.001(4)	0.000070(3)	0.000060(5)	$5.89 \cdot 10^{-5}$
	ZGR	3	4	0.0019(4)	0.0003(8)	0.000069(9)	$5.89 \cdot 10^{-5}$
4	RY1	6	6	0.005(8)	0.0000(6)	0.0000(2)	$2.13 \cdot 10^{-5}$
	RY2	9	9	0.006(8)	0.0002(2)	0.0000(8)	$1.72 \cdot 10^{-10}$
	ZGR	7	9	0.006(6)	0.000(1)	0.000019(1)	$1.73 \cdot 10^{-9}$
5	RY1	8	10	0.02(7)	0.0019(2)	0.001(7)	$1.47 \cdot 10^{-3}$
	RY2	12	16	0.02(5)	0.001(8)	0.003(4)	$4.51 \cdot 10^{-8}$
	ZGR	15	18	0.01(2)	0.002(6)	0.000013(5)	$6.23 \cdot 10^{-8}$
6	RY1	10	15	0.09(3)	0.007(4)	0.006(2)	$5.71 \cdot 10^{-3}$
	RY2	15	25	0.14(1)	0.003(8)	0.008(2)	$1.47 \cdot 10^{-5}$
	ZGR	31	35	0.10(1)	0.00(1)	0.00006(9)	$4.68 \cdot 10^{-8}$

Table 1: Ideal results of the simulations for the harmonic oscillator for each number of qubits (# qubits), ansatz and optimizer. The number of parameterers (# parameters) and the number of CNOT's of each ansatz for each number of qubits are shown. The infidelities for the COBYLA, SPSA and ADAM optimizer are the median of the infidelities over 100 simulations using Qiskit's Qasm simulator with 8192 evaluations. The L-BFGS-B optimizer is combined with the statevector simulator to establish the numerical limit of each ansatz.

# qubits	Ansatz	# parameters	# CNOT's	$1 - F^\infty$ COBYLA	$1 - F^\infty$ SPSA	$1 - F^\infty$ ADAM	$1 - F^\infty$ L-BFGS-B
2	RY1	2	1	0.159(5)	0.15907(4)	0.15910(0)	$1.59 \cdot 10^{-1}$
	RY2	3	1	0.1602(3)	0.15909(8)	0.15911(0)	$1.59 \cdot 10^{-1}$
	ZGR	1	1	0.159(2)	0.15906(5)	0.15917(8)	$1.59 \cdot 10^{-1}$
3	RY1	4	3	0.003(1)	0.00129(0)	0.00128(4)	$1.28 \cdot 10^{-3}$
	RY2	6	4	0.003(1)	0.00129(2)	0.001280(2)	$1.28 \cdot 10^{-3}$
	ZGR	3	4	0.0020(0)	0.00134(4)	0.001314(4)	$1.28 \cdot 10^{-3}$
4	RY1	6	6	0.007(9)	0.0001(8)	0.0001(2)	$1.06 \cdot 10^{-4}$
	RY2	9	9	0.010(1)	0.0005(7)	0.0001(9)	$5.67 \cdot 10^{-11}$
	ZGR	7	9	0.006(0)	0.000(5)	0.000109(6)	$5.78 \cdot 10^{-11}$
5	RY1	8	10	0.11(6)	0.008(1)	0.0066(3)	$6.15 \cdot 10^{-3}$
	RY2	12	16	0.12(5)	0.002(7)	0.001(8)	$1.51 \cdot 10^{-6}$
	ZGR	15	18	0.21(7)	0.01(0)	0.00022(7)	$1.47 \cdot 10^{-7}$
6	RY1	10	15	0.271(1)	0.01(9)	0.0140(7)	$1.30 \cdot 10^{-2}$
	RY2	15	25	0.22(2)	0.01(9)	0.010(6)	$3.44 \cdot 10^{-4}$
	ZGR	31	35	0.25(0)	0.2(0)	0.00031(4)	$1.49 \cdot 10^{-5}$

Table 2: Ideal results of the simulations for the transmon qubit for each number of qubits, ansatz and optimizer.